Chapter 4

Tracing temperature and radiation fields in TTs and HAe disks

Excerpts from this chapter were previously published in "Millimeter observations of HDO and DCN in the circumstellar disks of protostars LkCa 15, MWC 480 and HD 163296." in the conference proceedings, SFChem 2002: Chemistry as a Diagnostic of Star Formation, Waterloo, Ontario, Canada N2L 3G1. To be published by NRC Press, Ottawa, Canada, p. 55.

Abstract

Deuterium-to-hydrogen ratios are sensitive tracers of the conditions throughout the star formation process. In particular, observations of deuterium in disks can be used to constrain the location and timescales of comet formation. In this study, we searched for the deuterated species DCN and HDO toward the T Tauri protostar LkCa 15 and the Herbig Ae stars HD 163296 and MWC 480 using the Owens Valley Radio Observatory Millimeter Array. DCN was detected toward HD 163296 and HDO was detected toward LkCa 15 indicating column densities of 1.30×10^{12} cm^{-2} and 2.88×10^{15} cm^{-2}, respectively, for optically thin emission. Upper limits are given for column densities of DCN in LkCa 15 and HDO in HD 163296 and MWC 480. We also present the detection of H^{13}CN toward LkCa 15, which in combination with the upper limits obtained for DCN indicates D/H$_{DCN}$ $< 1.0\times10^{-3}$ for this disk. HCN has been searched for, but not detected, in HD 163296 (Qi, 2001) and the detection of DCN presented here indicates D/H$_{DCN}$ < 0.094 in this source. HDO/H$_2$O was estimated through comparison with predicted H$_2$O abundances from chemical models, scaled by the HCN(modeled)/HCN(observed) abundances. The resulting deuterium fractionations in LkCa 15 and HD 163296 were found to be similar to those found toward the T Tauri star disk TW Hya and those observed in molecular clouds and hot cores. The structure of the HDO emission toward LkCa 15 was modeled and is discussed in this chapter.

4.1 Introduction

Changes in the composition of ice and gas during the process of planet formation likely lead to the rich diversity of planetary systems discussed in Chapter 1. Observations tracing the evolution of material in young stellar objects (YSOs) are also essential for addressing issues such as the formation of comets and the origin of life. The ratio of deuteron-bearing to hydrogen-bearing forms of a species (D/H) can be indicative of the physical and chemical evolution during the star formation process. D/H ratios have been measured for several objects in our solar system, including planets, comets and meteorites, as well as presolar analogues like hot cores and molecular clouds. As Figure 4.1 shows, these observations indicate that deuterium abundance is a sensitive tracer of the changes in the composition of circumstellar material that occur throughout (pre)stellar evolution; the D/H ratio decreases by orders of magnitude from molecular clouds to hot cores to the presolar nebula. Thus, the comparison of the D/H ratios in these stages of star formation (i.e., the comparison of protoplanetary disks with comets and Kuiper Belt objects) will allow us to take full advantage of YSOs as a laboratory in which to study the chemical and physical properties of our own Solar System in its infancy and to investigate the origin of primitive solar system bodies.

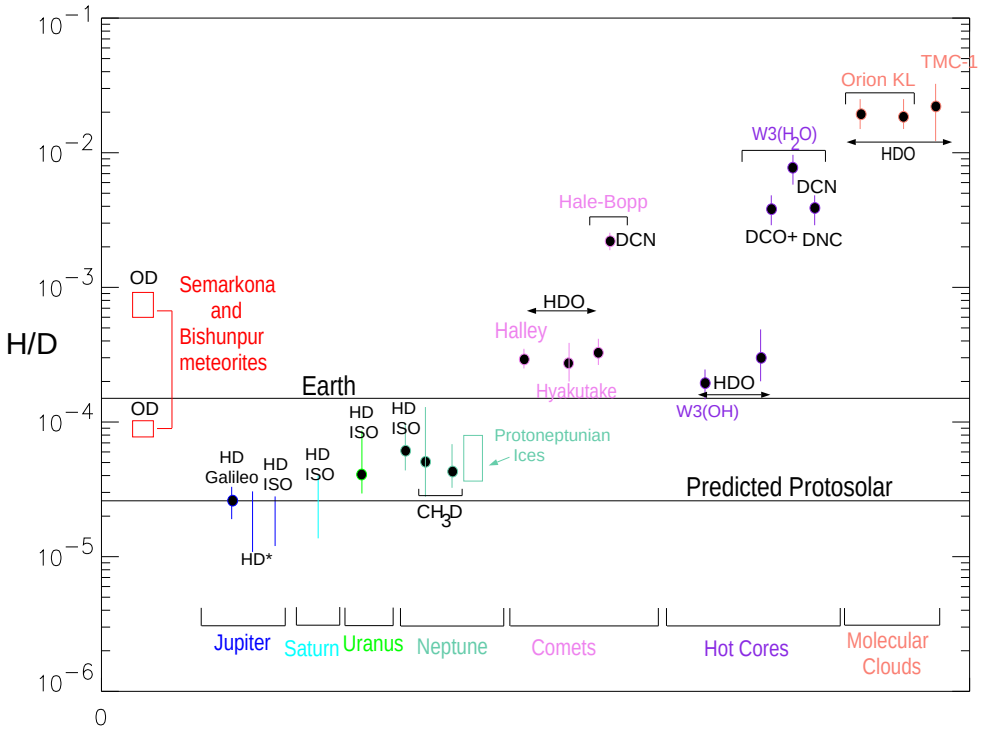

Figure 4.1 This graph is modeled after that presented in Bockelée-Morvan et al. (1998) and Drouart et al. (1999) (see these papers for a review of observations of solar system objects). The deuterium abundances for hot cores (Mangum 1991; Helmich et al., 1996) and molecular clouds (Mangum et al., 1991; Wootten, 1987) were added for comparison with that found for the accretion disks encircling LkCa 15, HD 163296 and MWC 480 studied here.

It is the strong dependence of deuterium enrichment on fractional ionization and temperature that makes the ratio of deuterium-to-hydrogen a particularly sensitive tracer of evolving physical conditions during the star formation process. The D/H ratio in the local ISM has been found to be (1.4–2.2)$\times 10^{-5}$ (Linsky et al., 1995; Linsky & Wood, 1996; Piskunov et al., 1997) and is consistent with the estimated protosolar D/H value of $\sim 1.6 \times 10^{-5}$ (as calculated from the conversion of D to ^{3}He in the solar wind; Gautier & Morel, 1997). Observations of cold molecular clouds indicate deuterium enrichments as high as D/H$\sim$0.01–0.05 (Wootten, 1987), however. Gas-phase chemical models of molecular clouds suggest that deuterium is enriched as a result of rapid ion exchange reactions, the most important of which are

$$H_3^+ + HD \rightleftharpoons H_2D^+ + H_2 \tag{4.1}$$

$$CH_3^+ + HD \rightleftharpoons CH_2D^+ + H_2 \tag{4.2}$$

$$C_2H_2^+ + HD \rightleftharpoons C_2HD^+ + H_2 \tag{4.3}$$

The difference in the zero-point energies of H- and D-bearing species is typically 100–400 K. For the reactions above, this small difference makes the reactions highly temperature dependent under the conditions prevailing in molecular clouds. High temperatures will overcome the modest endothermicities and push these reactions to the left, decreasing production of the deuterated species, but at the low temperatures (T $<$ 20 K) of dense molecular cloud cores, the reactions proceed efficiently to the right. In these cold environments, depletion onto grain surfaces may also enhance the deuterium enrichment. As neutral species are depleted from the gas through accretion onto grain surfaces the primary destruction mechanism for deuterated ions is blocked and the D/H ratios in the gas phase increase (Brown & Millar, 1989). The presence of ionized species, such as H_3^+ and H_2D^+, is highly dependent on the abundance of atoms or molecules such as CO, O and N_2, which have a proton affinity greater than that of H_2. The abundances of these neutral species are largely dependent on the degree of depletion onto grain surfaces. The combination of these two effects is the most likely cause of the observed cloud-to-cloud variations in deuterium enrichment, where decreasing deuterium enrichment can be associated with increasing cloud temperature (Wootten, 1987).

Observations of deuterated species in hot cores (Jacq et al., 1990; Helmich et al., 1996; Gensheimer et al., 1996) find $(D/H)_{H_2O}$ of (1–3)$\times 10^{-4}$ and $(D/H)_{HCN}$ of (5–8)$\times 10^{-3}$, much higher than expected due to their temperature (T $\approx$ 200 K). These results were initially puzzling, but were later explained by models in which the gas-phase abundances in hot cores result directly from evaporation of largely unprocessed interstellar material, which has previously been frozen out onto grain mantles (Walmsley et al., 1987; Brown et al., 1988). Although grain surface reactions occur, the D/H ratio is not expected to change considerably, because the mobility of deuterium atoms on grain surfaces is similar to that of hydrogen (which scans a 0.05 μm grain in $\sim 1 \times 10^{-7}$ s; Brown & Millar,

1989). The degree of enrichment in hot cores thus reflects that in molecular clouds prior to accretion onto grain surfaces. Only after a significant amount of time, models suggest $\sim 10^5$yr (Brown et al., 1988), are gas-phase reactions believed to significantly affect the deuterium abundances due to the very large initial D/H ratios of grain mantle ejecta.

For some molecules, ion exchange reactions like those discussed above are slow and the main source of deuterium enrichment is ion-molecule and deuteron exchange reactions with heavily deuterated parent molecules (Millar et al., 1989). The efficiency of ion-molecule reactions, and the ionization rate, thus also affects the degree of deuterium enrichment. Observations indicate that D/H ratios in hot cores and molecular clouds are much larger than that of the early solar nebula ($\sim 10^{-5}$), where ion-molecule reactions as well as neutral-neutral reactions are important. Direct measurements of D/H in disks can therefore greatly improve our understanding the chemistry occurring in this nebular stage, particularly if they resolve the disk probing radial variations in the D/H ratio. If neutral-neutral reactions dominate (Geiss & Reeves, 1981), then D/H enrichments higher than a factor of a few are difficult to obtain. However, more recent chemical models (Finocchi et al., 1997; Willacy & Langer, 2000; Aikawa et al., 2002) indicate that ion-molecule reactions play an important role in disk chemistry because cosmic rays and X-rays increase the ionization rate (to $\geq 10^{-17}$ s^{-1}) and thus the importance of ion-molecule reactions. Additionally, the effectiveness of deuteron transfer reactions in altering the deuterium enrichment is dependent on the mixing processes in disks, which are in turn controlled by the ionization of the gas (Aikawa & Herbst, 2001). Evaporation from and recondensation onto grain surfaces will likely occur repeatedly in disks thanks to mixing and processes such as grain-grain collisions. Therefore, measurements of deuterated molecules in disks can constrain the importance of ion-molecule reactions and ionization in disks and possibly explain the apparent decrease in D/H ratio during stellar and planetary evolution.

Comparison of the deuterium enrichment in each stage of star and planet formation with that of comets and meteorites can also be used to gain a more complete understanding of the formation of small bodies in our solar system. As noted above, molecules in cold clouds are enriched in deuterium relative to the ISM. This notable deuterium enrichment in molecular clouds and the moderate enrichment in comets, $\sim 2\times 10^{-3}$ for DCN/HCN and $\sim 3\times 10^{-4}$ for HDO/H_2O, has been interpreted as a possible indication of interstellar versus nebular cometary origins (Eberhardt et al., 1995; Bockelée-Morvan et al., 1998; Meier et al., 1998a). However, recent models of chemistry in circumstellar accretion disks (Aikawa & Herbst, 1999; Aikawa & Herbst, 2001) suggest that the deuterium fractionation changes significantly during the collapse of the molecular clouds and during the accretion process itself. So, although the D/H ratios of comets are similar to that of molecular clouds, it is not likely that comets are formed of truly "pristine" interstellar material. Their composition should, in fact, be strongly dependent on the structure of the circumstellar disk in which they were assembled.

Temperatures and densities in circumstellar disks are thought to vary strongly as a function of radius and height, and detailed chemical models (Willacy & Langer, 2000; Aikawa et al., 2002) predict that these gradients should be reflected in molecular abundances–as can be seen in the measured D/H ratios of the solar system. Most solar system objects, including planets, protoneptunian ices and the majority of carbonaceous meteorites, appear to have been formed in a reservoir with deuterium content (D/H $< 9 \times 10^{-5}$) similar to the accepted protosolar value. However, the presence of a minor component of the sample of carbonaceous meteorites with a much larger D/H ratio $\approx 7 \times 10^{-4}$ (Deloule et al., 1997) indicates that the solar nebula was most likely heterogeneous and suggests the presence of reservoirs in which there was substantial deuterium enrichment.

The effects of nebular heterogeneity should also be visible in the deuterium content of comets. Although the origin of comets is currently not well understood, measurements of D/H ratios in comets should help clarify the physical and chemical conditions under which they formed. It has been proposed that short-period comets originated in a cold (T$\sim$25 K) region beyond Neptune's orbit (Kuiper, 1951; Duncan et al., 1988; Fernandez & Ip, 1991; Festou et al., 1993) and that long-period comets formed in a warmer outer-planet region (from Jupiter to Neptune) and were then dynamically scattered into the Oort cloud by interactions with Jupiter (Eberhardt et al., 1995). The difference in the physical conditions (particularly temperature) of the formation regions for these two types of comets should be evident in their chemical and isotopic composition, with Kuiper belt comets possessing a more "interstellar" composition and Oort cloud comets more closely resembling the solar nebula (Eberhardt et al., 1995).

The deuterium fractionation in comets Halley, Hayukutake and Hale-Bopp, believed to be Oort cloud comets, has been observed to be intermediate between that of the early solar nebula and that of cold molecular clouds; DCN/HCN in Hale-Bopp is $\sim 2 \times 10^{-3}$ (Meier et al., 1998a) and HDO/H_2O is $\sim 3 \times 10^{-4}$ in Haley, Hayukutake and Hale-Bopp (Eberhardt et al., 1995; Bockelée-Morvan et al., 1998; Meier et al., 1998b). To date, deuterated species have not been observed in short-period comets. However, as discussed by Rodgers & Charnley (2002), the comets Linear S4 (believed to have originated near Jupiter in the protosolar nebula) and Giacobini-Zinner (thought to be a Kuiper belt object) have chemistry which deviates from the "norm", including large (factors as high as $\sim$15) depletions of volatile carbon-chain molecules, (Weaver et al., 1999, Mumma et al., 2001) indicating that chemical composition of comets may indeed be dependent on their place of origin.

It is clear that a better understanding of the role of deuterium fractionation in stellar evolution and comet formation is dependent upon the development of a detailed model of nebular conditions. Observations of circumstellar disks around other protostars provide an opportunity to directly study environments that may be similar to the early stages of our Solar System. Recently, millimeter-wave interferometers have imaged disks of gas and dust surrounding several young T Tauri and Herbig Ae/Be stars (see Beckwith & Sargent, 1996 for a review) resulting in dramatically improved models

Table 4.1. Stellar properties of observed sources.

Star colhead	R.A. (1950)	Dec. (1950)	SpT	d (pc)	T_{eff} (K)	R_* ($R_\odot$)	L_* ($L_\odot$)	M_* ($M_\odot$)	Age (Myr)	V_{ref} (km/s)
LkCa 15	04 36 18.40	+22 15 11.6	K7	140	4365	1.64	0.72	0.81	11.7	6.0
HD 163296	17 53 20.61	-21 56 57.3	A3Ve	122	9550	2.2	30.2	2.3	6	6.0
MWC 480	04 55 35.69	+29 46 05.7	A3ep+sh	131	8710	2.1	32.4	2	4.6	5.1

of disk physical and chemical structure. Among the characteristics now under study, disk geometry, velocity structure, dust and gas masses, fractional ionization, temperature distributions, and the degree of depletion of gas-phase species onto grain surfaces have now been examined in a handful of sources (Dutrey et al., 1997; Qi, 2001; Simon et al., 2001; Dartois et al., 2003; Qi et al., 2003). Observations of deuterated species in circumstellar disks are particularly exciting, in that they should directly constrain the (D/H) fractionation in the outer (low temperature) regions of these disks. The accretion in protoplanetary disks is largely viscous; material spirals inward toward the star at a typical accretion rate of 10^{-8} $M_\odot$/yr and by the end of the accretion phase material which was at radii of hundreds of AU from the star now resides in the comet-forming region. When combined with the previously obtained information about disk structure, the observed deuterium fractionation in the outer disk can be directly compared to that in comets and in the ISM to more fully understand comet formation.

In this study, the deuterated species DCN and HDO were observed toward the disks surrounding LkCa 15, a T Tauri star, and HD 163296 and MWC 480, Herbig Ae stars, using the Owens Valley Radio Observatory (OVRO) Millimeter Array. These sources were previously identified through ^{12}CO observations to possess circumstellar material with Keplerian velocity structure (Beckwith & Sargent, 1996; Mannings & Sargent, 1997), except for HD 163296 for which the velocity field has not yet been modeled in detail. These objects were also found to be strongly emitting in initial molecular line observations of HCN 1-0, HCO^+ 1-0 and CN 1-0 and are part of a larger survey of molecular line observations in circumstellar accretion disks, in which the dominant chemical species in the C,N,O,S-budgets are being observed (Qi, 2001; Qi et al., 2003; this thesis). Stellar and disk parameters for these three sources are presented in Table 4.1.

The observations will be presented in §2. In §3, the deuterium fractionation will be evaluated in each disk through the comparison of the observed DCN abundances with those found for HCN and H^{13}CN and of the observed HDO abundances with H_2O abundances predicted by chemical models, scaled by the CO(predicted)/CO(observed) or HCN(predicted)/HCN(observed) abundances of the disks in our sample. The observed deuterium fractionation in these three disks will be compared to those obtained via chemical models and those observed for molecular clouds, hot cores, comets and solar system objects in §4.

Table 4.2. Observational parameters

Source	Molecule	Transition	ν (GHz)	Θ (arcsec)	configuration(s)	$\int T_A^* dv$ (K km/s)	N_i (cm^{-2})
LkCa15	HDO	1_{11}-2_{12}	225.8967	2.16×2.10	C+L+H	4.94	7.25(15)
-	HDO	3_{12}-2_{11}	241.5615	1.43×1.18	C+L+H	18.1	4.24(15)
-	DCN	3-2	217.2386	3.24×1.78	L+E+C	<3.01	<3.06(12)
-	$H^{13}CN$	3-2	259.0118	0.87×0.72	H	65.1	5.34(13)
-	$H_2{}^{18}O$	3_{13}-2_{20}	203.4075	2.71×1.25	E+C	<3.01	<3.23(16)
HD 163296	HDO	1_{11}-2_{12}	225.8967	1.78×1.23	L+H	<188	<2.76(17)
-	DCN	3-2	217.2386	3.58×2.24	L+E	1.04	1.30(12)
MWC 480	HDO	1_{11}-2_{12}	225.8967	4.60×2.50	C+L	0.285	4.18(14)

4.2 Observations

The observations were made using the Owens Valley Radio Observatory (OVRO) Millimeter Array[1]at Big Pine, California, between October 1997 and March 2002. The sources were observed in combinations of the C, L, E and H configurations of the array. The beam sizes and receiver tunings for the observed transitions toward each source are shown in Table 4.2. Average single sideband system temperatures ranged from 400–750 K. The bandpass was calibrated using a boxcar fit to an internal noise source modified by a second order polynomial fit to observations of an astronomical source; either 3C84, 3C454.3, 3C345, 3C279 or 3C273 were used subject to availability at the time of observation. Observations of a phase and amplitude calibrator were interleaved with source observations approximately every half hour, using 3C111 and 0528+134 for LkCa 15, NRAO 530 for HD 163296 and 0538+134 for MWC 480. The flux density scale was established from concurrent observations of Neptune and Uranus during their transit or the quasars used for bandpass calibration, whose fluxes were found by "boot-strapping" from ∼concurrent planet observations. Bandpass, phase and flux calibrations were applied to the data with the MMA software package (Scoville et al., 1993). Subsequent imaging and spectral analysis were performed using the MIRIAD data reduction software package (Sault et al., 1995).

4.3 Column densities and D/H ratios

Gaussian fits to the observed emission lines were used to obtain the integrated intensities ($\int T_A^* dv$) shown in Table 4.2. If emission was not detected, the rms noise level obtained in the observations (Table 4.2) was used to calculate an upper limit for the integrated intensity by assuming a line width at the 1σ level that was consistent with observed line widths of the ^{13}CO 1-0 transition toward these sources (Qi, 2001; Duvert et al., 2000; Mannings & Sargent, 1997) and calculating the integrated intensity at 3σ. In all cases, the column densities were then calculated from the integrated intensities

[1]OVRO observations were supported by the National Science Foundation, AST 9981546.

using the following relation, assuming that the emission is optically thin,

$$\int T_A^* dv = \frac{8\pi}{3k}\nu\mu^2 S \frac{N_T}{Q(T_{ex})} e^{-E_u/kT_{ex}}, \tag{4.4}$$

where S is the line strength and was obtained from integrated intensities (I_{cat}) of the emission lines in laboratory spectra at a temperature ($T_0 = 300$ K) as reported in the JPL Molecular Spectroscopy on-line catalog (Pickett et al., 1998) by,

$$I_{cat} = \frac{8\pi}{3h}\mu^2 S \frac{\langle e^{-E_l/kT_0} - e^{-E_u/kT_0}\rangle}{Q(T_0)}. \tag{4.5}$$

In the two equations above, N_T is the total column density in cm^{-2}, Q is the rotational partition function, E_u and E_l are the energies (in ergs) of the upper and lower states, ν is the transition frequency (Hz), μ is the permanent dipole moment, h is the Planck constant and k is the Boltzmann constant.

In addition, it was assumed that the emitting region is in Local Thermal Equilibrium (LTE) and approximately isothermal with $T_K = T_{ex} = 30$ K. The assumption of LTE may not be valid, especially for water, as most of the emission is thought to arise near the superheated disk surface (van Zadelhoff et al., 2001), and a more detailed, non-LTE analysis is being pursued in a separate study (Chapter 2). An isothermal disk with temperature 30 K is appropriate for the outer radii (70 $< R <$ 400 AU) of the disks to which we are sensitive at millimeter wavelengths (D'Alessio et al., 1999). The resulting column densities and upper limits are presented in Table 4.2.

DCN was detected toward the Herbig Ae star HD 163296, with a column density of 1.30×10^{12} cm^{-2} (Figure 4.2). Only one L track was obtained, however, and the poor (u, v) sampling resulted in the triple peaked integrated intensity map shown in Figure 4.2. This is similar to that seen for the continuum radiation toward HD 163296 in the same observations and is not believed to be the true structure of the DCN emission. The left panel of Figure 4.2 shows the continuum emission (in color scale) overlaid with continuum+DCN emission for HD 163296. Although the map is clearly dominated by the strong 1 mm continuum, spectra of the left, middle and right lobes reveal detectable DCN emission. The velocity of the DCN emission (right panel) matches that seen for CO 2-1 (Mannings & Sargent, 2000). This detection of DCN was unexpected because HCN was not seen toward this source, restricting the column density of HCN to $<1.1\times10^{13}$ cm^{-2}. Assuming the highest DCN/HCN ratio seen in molecular clouds, $\sim2.0\times10^{-2}$, we would expect a column density of DCN of $\leq2.2\times10^{11}$, or an integrated intensity of $\times10^{-4}$ K km/s. HDO was not detected toward HD 163296 and upper limits of 6.96×10^{15} cm^{-2} were obtained.

Toward LkCa 15, both the HDO 1_{11}-2_{12} and 3_{12}-2_{11} transitions were marginally detected and yield column densities of 4-7.25×10^{15} cm^{-2} (Figure 4.3). The integrated intensity map for the HDO

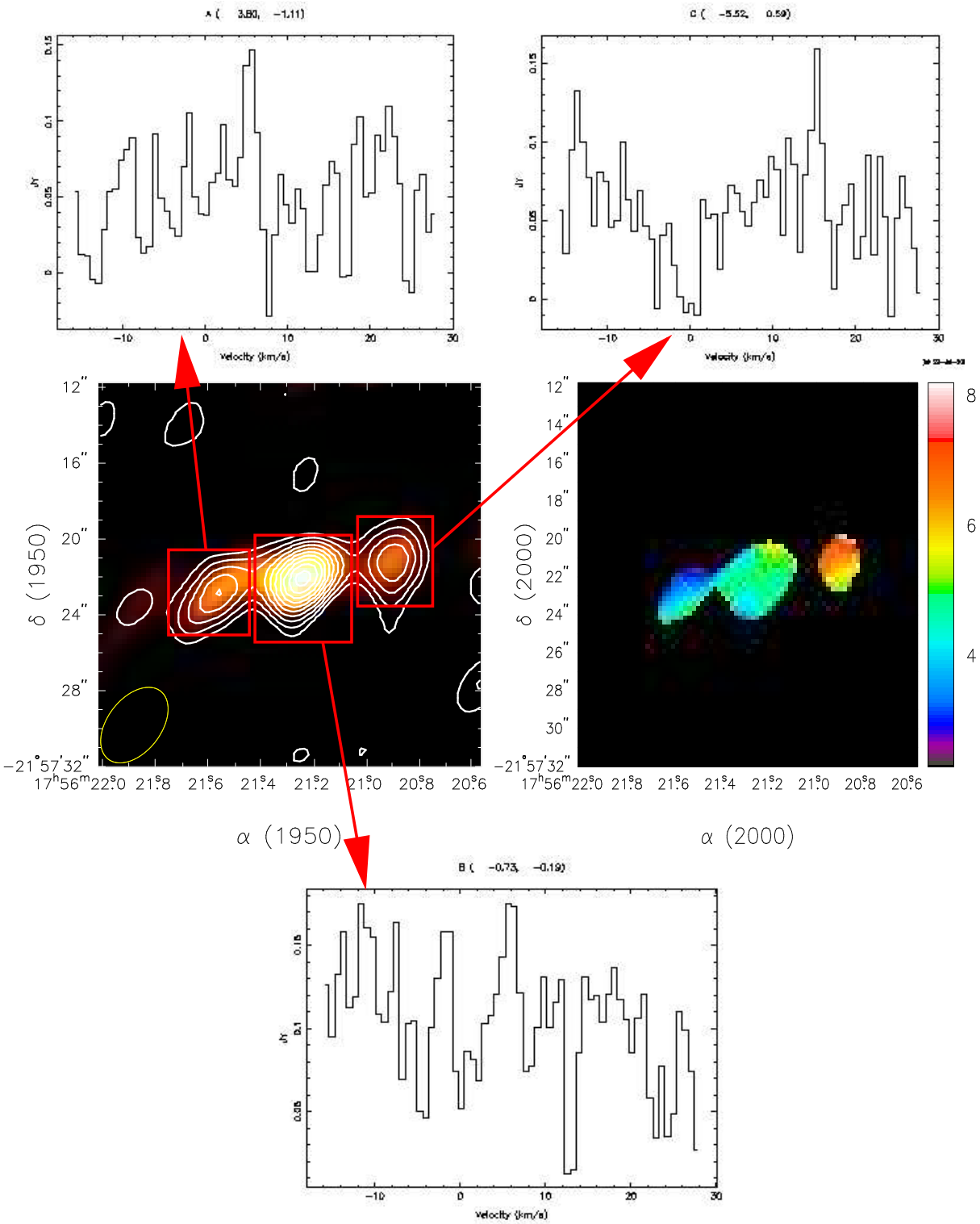

Figure 4.2 DCN 3-2 emission from HD 163296. The left panel shows the continuum emission (in color scale) overlaid with continuum+DCN emission (contours), with contours spaced by 1σ starting at 1σ. The color scale starts at 3σ. Spectra of the left, middle and right lobes are shown as indicated. The right panel shows the moment 1, or velocity map, that matches that seen in CO 2-1 (Mannings & Sargent, 2000).

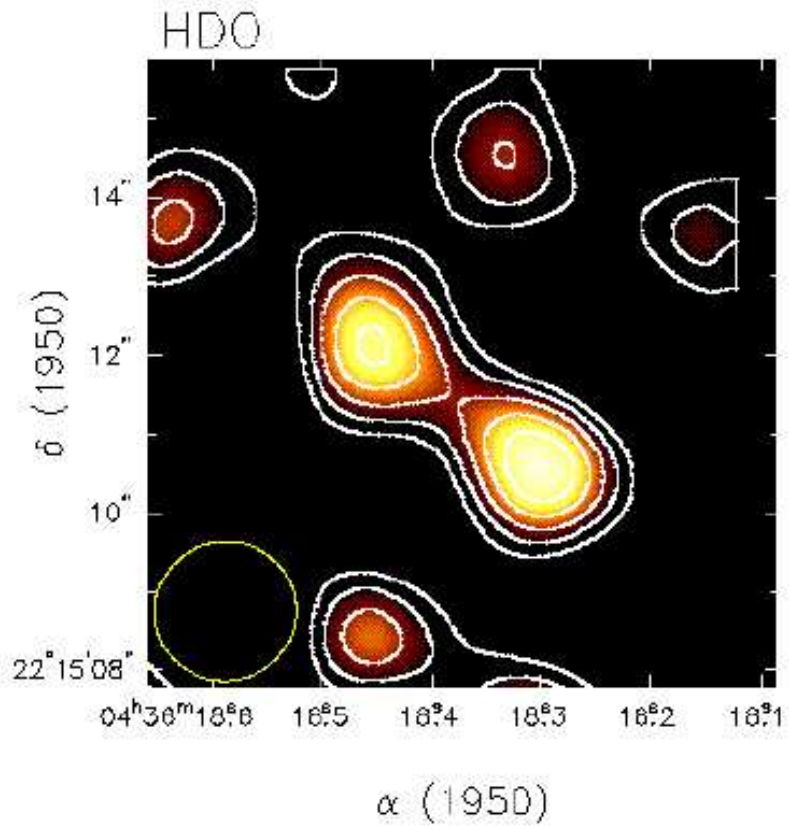

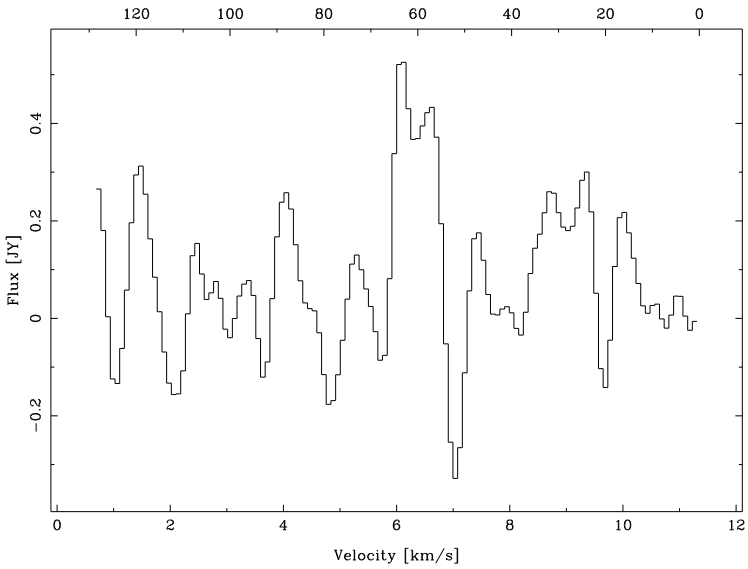

Figure 4.3 HDO 1_{11}-2_{12} emission from LkCa 15. The top panel shows the integrated intensity map, with contours starting at 0.5σ and spaced by 0.5σ to emphasize the spatial distribution of the emission, which is quite similar to that of HCN toward this source. The spectrum in a $4'' \times 4''$ box is shown in the lower panel.

1_{11}-2_{12} emission depicts two peaks approximately 2" away from the continuum (stellar) position, located along the major axis of the disk. Although the emission is weak, the spectral line shape and the velocity distribution of the HDO emission is similar to that of previously observed for CO 2-1 toward this source (Qi et al., 2003), indicating that it does arise from disk material. The spatial distribution of the HDO emission is quite similar to the morphology of the CN and HCN emission toward this source and can be simulated by emission from an annulus of gas extending from R = 200–400 AU (§6). $H_2{}^{18}O$ was not detected toward LkCa 15 and we use the upper limit to the column density of $H_2{}^{18}O$ (1.25×10^{16} cm^{-2}) and the typical $^{16}O/^{18}O$ ratio for the local ISM (560±25; Wilson & Rood, 1994) to find an upper limit to the water column density of 7.0×10^{18} cm^{-2} in order to derive a D/H ratio. DCN was not detected toward LkCa 15 and upper limits for DCN (of 5.40×10^{11} cm^{-2}) were obtained. $H^{13}CN$ was detected toward LkCa 15 (Figure 4.4) at a column density of 9.23×10^{12} cm^{-2} and will be used in combination with the upper limits obtained for DCN to calculate a DCN/HCN ratio in LkCa 15. HDO was not detected toward MWC 480, resulting in an upper limit of 3.66×10^{15} cm^{-2}.

The $(D/H)_{HCN}$ ratio can be calculated directly from the DCN abundances presented here and previous observations of HCN in LkCa 15 and HD 163296 (Qi, 2001). For LkCa 15, HCN 1-0 emission was observed to be optically thick, and therefore the column density of $H^{13}CN$ measured here and the interstellar $^{13}C/^{12}C$ ratio of 60 were used to estimate the HCN abundance of 5.5×10^{14} cm^{-2}. For HD 163296, HCN was not detected (Qi, 2001) so an upper limit of 1.1×10^{13} cm^{-2} for HCN was used, as derived from an optically thin, LTE calculation. The resulting $(D/H)_{HCN}$ ratios in the disks around LkCa 15 and HD 163296 are $<2\times10^{-3}$ and > 0.176, respectively. Because water has not been detected toward these three sources, the calculation of the $(D/H)_{H_2O}$ is not as straightforward as that of $(D/H)_{HCN}$. For these reasons, the HDO abundances obtained from our observations are most useful when compared with model predictions.

4.4 Chemical models of circumstellar disks

Extensive chemical modeling of disk chemistry has been pursued by Aikawa et al. (1999) and Willacy & Langer (2000). These models predict molecular abundances as a function of height and radius in disks of ages ranging from 1–10 Myr. Although the physical models used by these two groups differ, both disk models assume that the gas is in hydrostatic equilibrium in the vertical direction and derive temperature and hydrogen density distributions that are similar. Aikawa et al. (1999) adopt the Kyoto model (Hayashi, 1981) for the physical disk structure, extrapolating to a radius of 700 AU and scaling the mass and density by an order of magnitude; whereas Willacy & Langer (2000) use the physical model of Chiang & Goldreich (1997), extrapolated to an outer radius of 1000 AU. The two models mainly differ in the treatment of grain surface reactions; Willacy & Langer (2000)

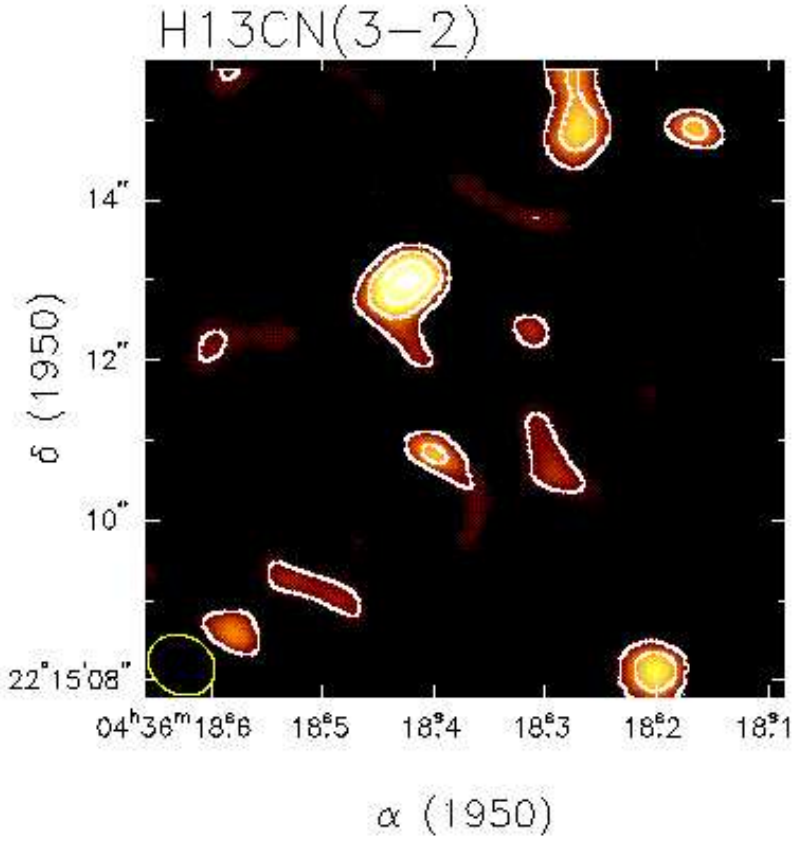

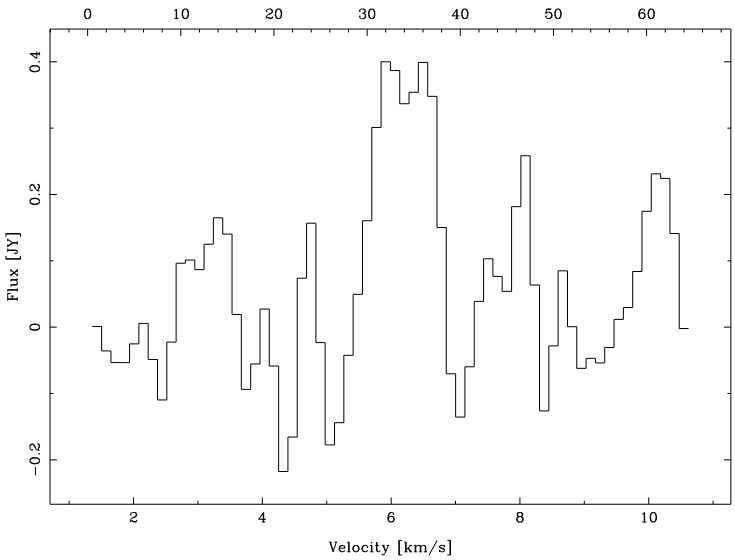

Figure 4.4 $H^{13}CN$ 3-2 emission from LkCa 15. The top panel shows the integrated intensity map of the emission, both contours and color scale, with contours starting at 1σ. The map is over-resolved as the data consists of only one H track, with a resolution of $\sim$1.5" and poor (u, v) coverage near the origin. An emission line can be seen in the spectrum taken at the stellar position over a box of size $1'' \times 1''$, shown in the lower panel.

include detailed surface chemistry while Aikawa et al. (1999) only include surface formation of H_2 molecules and recombination of ions and electrons and adopt an artificially low sticking probability S = 0.03 instead of the detailed treatment of non-thermal desorption performed by Willacy & Langer (2000). These differences affect the molecular distributions as functions of disk height and radius, but do not greatly effect the average abundances of the major species, including CO, CN, HCN, and HCO^+, which are consistent with the observed abundances of these species in disks (e.g., DM Tau, Guilloteau & Dutrey, 1998; Dutrey et al., 1997; L1157, Goldsmith et al., 1999).

Recently, chemical models of disks have been expanded to include singly deuterated molecules by assuming that the reaction rates are identical to their hydrogen-bearing counterparts (Aikawa & Herbst, 2001; Aikawa et al., 2002). The chemical reactions involving these deuterated molecules include normal exothermic and dissociative recombination reactions (assuming statistical branching ratios) and a subset of deuterium exchange reactions, involving molecular ions and HD, that are predicted to proceed in disks based on theoretical or laboratory studies. Additionally, Aikawa et al. (2002) incorporate a vertical temperature gradient as calculated by D'Alessio et al. (1999). This is the first detailed disk chemical model including deuterated molecules and so will be used for comparison with our observations, although we note that (as discussed above) this model does not include a detailed treatment of grain surface reactions or non-thermal desorption mechanisms.

This model suggests that deuterium fractionation in disks should be similar to that in molecular clouds, beginning with the enrichment through rapid ion exchange reactions and then propagating to other molecules, primarily through ion-molecule chemistry (Millar et al., 1989). Additionally, if the molecular ions which are enriched in deuterium undergo dissociative electron recombination, resulting in a high atomic D/H ratio, then the deuterium enrichment can propagate via neutral-neutral reactions. The distribution of HDO and DCN in disks is determined primarily by the specific formation mechanisms of these species. The Aikawa & Herbst (1999) model predicts that HDO is formed via formation of H_2DO^+ in the following reaction network:

$$CH_4D^+ + O \rightarrow H_2DO^+ + CH_2 \tag{4.6}$$

$$H_2O + H_2D^+ \rightarrow H_2DO^+ + H_2 \tag{4.7}$$

$$H_2D^+ + O \rightarrow OD^+ + H_2 \rightarrow HDO^+ \xrightarrow{H_2} H_2DO^+ + H \tag{4.8}$$

$$H_2DO^+ + e^- \rightarrow HDO + H. \tag{4.9}$$

Thus, the production of H_2D^+ is pivotal in the formation of HDO. Because the reaction H_3^+ + HD $\rightleftharpoons$ H_2D^+ + H_2 is very sensitive to temperature, the HDO/H_2O ratio will increase dramatically at larger radii and colder temperatures. Near the midplane, depletion of neutral molecules, CO in

particular, leads to increased deuterium enrichment as the reactions $H_2D^+ + CO \rightarrow DCO^+ + H_2$ and $H_2D^+ + CO \rightarrow HCO^+ + HD$ are the dominant destruction mechanisms for H_2D^+ at high densities, versus electron recombination or reaction with H_2 at low densities. HDO is therefore predicted to increase as a function of radius in the disk (peaking near R$\sim$200 AU), due to reduced production of HDO near the central star as H_2D^+, the primary precursor to HDO, is destroyed. This scenario naturally explains the double peaked HDO emission observed here (Figure 4.3).

The production of DCN is complicated by the fact that several ion-molecule reactions do not produce a statistical balance of deuterated and H-bearing products:

$$HCN + H_2DO^+ \rightarrow HCND^+ + H_2O \tag{4.10}$$

$$HCN + H_2DO^+ \rightarrow HCNH^+ + HDO \tag{4.11}$$

$$HCN + H_2DO^+ \not\rightarrow DCNH^+ + HDO \tag{4.12}$$

$$HCND^+ + e^- \rightarrow HCN + D \tag{4.13}$$

$$HCND^+ + e^- \not\rightarrow DCN + H. \tag{4.14}$$

Thus, the primary mechanisms for production of DCN involve the grain-surface reactions,

$$(a) \quad H_2CN + D \rightarrow HCN + HD \tag{4.15}$$

$$(b) \quad H_2CN + D \rightarrow DCN + H_2, \tag{4.16}$$

with a branching ratio (a:b) of 5$\pm$3 (by experiment; Nesbitt et al., 1990), and the gas-phase reactions

$$CH_2D^+ + N \rightarrow DCN^+ + H_2 \tag{4.17}$$

$$DCN^+ + e^- \rightarrow DCN \tag{4.18}$$

$$DCN^+ + H_2 \rightarrow DCNH^+ + H \tag{4.19}$$

$$DCNH^+ + e^- \rightarrow DCN + H. \tag{4.20}$$

Reactions 4.15, 4.16 and 4.17 are dependent on the grain surface formation of H_2CN and hydrocarbons (CH_4 and CH_3), respectively, and on the subsequent desorption of these molecules into the gas phase. Thus the DCN/HCN ratio is therefore expected to peak at warmer temperatures than the HDO/H_2O ratio, and so Aikawa & Herbst (2001) predict that HDO and DCN will have differing distributions as a function of radius and height (c.f. Figure 2 in Aikawa & Herbst, 2001).

Aikawa et al. (2002) note that D/H ratios should increase with total disk mass, due to increased depletion of molecules onto grain surfaces. For this reason, it is important that the model predictions

are scaled by the masses of the three disks in our sample. We simplify this by scaling the deuterated molecule abundances from Aikawa et al. (2002) by the observed abundances. For DCN, we scale by the observed abundance of HCN,

$$N_{DCN}(predicted) = (D/H)_{HCN}(modeled) \times N_{HCN}(observed) \tag{4.21}$$

Because H_2O has not been observed for the disks in our sample, another proxy for the disk mass is required. CO is often used as a proxy for H_2 and the total disk mass. However, disk masses derived from CO isotopomers with standard dense cloud abundances were up to two orders of magnitude less than the minimum mass inferred from dust emission (Beckwith et al., 1990; Qi, 2001). This is likely due to strong depletion of CO onto grain surfaces. Additionally, previous observations of LkCa 15 (Qi et al., 2003) indicate although the predictions of Aikawa & Herbst (2001) for CO and HCO^+ are close to the observed quantities, those for CN and HCN disagree by up to 2 orders of magnitude. In the calculation of N_{HDO}(predicted) we therefore use both the observed CO and HCN abundances as proxies for the disk mass and scale by the ratio of the observed-to-modeled abundances for each.

$$N_{HDO}(predicted) = N_{HDO}(modeled) \times N_{HCN}(observed)/N_{HCN}(modeled) \tag{4.22}$$

$$N_{HDO}(predicted) = N_{HDO}(modeled) \times N_{CO}(observed)/N_{CO}(modeled) \tag{4.23}$$

Using the modeled abundances of DCN, HCN, HDO and CO and previously observed column densities of HCN and CO in the disks in our sample (Qi, 2001), we can predict the column densities of DCN and HDO that are required to be consistent with the Aikawa et al. (2002) model. The modeled column densities are presented in Table 4.3. These are average abundances obtained from Aikawa et al., 2002 for radii from 100 AU to 400 AU, where the outer radius is consistent with CO observations toward LkCa 15, HD 163296 and MWC 480 (Qi, 2001; Table 4.1). As the ^{12}CO and HCN J=1-0 transitions are expected to be optically thick, Qi (2001) obtained ^{12}CO and H^{12}CN abundances from observations of ^{13}CO 1-0, C^{18}O 1-0, HCN 1-0 and H^{13}CN 1-0. In our calculations the rarest isotope detected for each species was used to calculate its molecular abundance, and interstellar ^{12}C/^{13}C and ^{12}C/^{18}C ratios of 60 and 500 were applied (Table 4.3).

The resulting predictions for the column densities of DCN and HDO for the disks in our sample are close to the observed column densities (Table 4.4) for HDO and DCN where the modeled abundances have been scaled by HCN abundances as calculated from the observed H^{13}CN 1-0 emission. This indicates that HCN 1-0 is optically thick in these disks, and that H^{13}CN 1-0 is a better tracer of the disk mass. This is confirmed by single dish observations of LkCa 15 and a one-dimensional LVG analysis of HCN 1-0 and H^{13}CN 1-0 (van Zadelhoff et al., 2001). The column densities of HDO are underestimated by two orders of magnitude when scaled by the CO column density inferred

Table 4.3. CO and HCN column densities.

Star	N_{HCN}(obs)	N_{CO}(obs)
LkCa 15	5.34×10^{13}[c]	1.65×10^{18}[a]
HD 163296	1.38×10^{13}	1.35×10^{18}[b]
MWC 480	4.07×10^{13}[c]	1.39×10^{18}[b]

[a]from $C^{18}O$ 1-0 observations

[b]from ^{13}CO 1-0 observations

[c]from $H^{13}CN$ 1-0 observations

Note. — Observed column densities were obtained from Qi (2001), with the exception of the $H^{13}CN$ 1-0 observations toward LkCa 15 presented in this chapter.

Table 4.4. Observed and predicted column densities.

Star	N_{HDO}(obs)	N_{HDO}(pred)	N_{DCN}(obs)	N_{DCN}(pred)
LkCa 15	5.74×10^{15}	2×10^{13}[a]-3×10^{15}[b]	$<3.06\times10^{12}$	2×10^{13}
HD 163296	$<2.76\times10^{17}$	1×10^{13}[a]-6×10^{13}[b]	1.30×10^{12}	3×10^{11}
MWC 480	4.18×10^{14}	1×10^{13}[a]-9×10^{15}[b]	-	5×10^{13}

[a]Predicted using $N_{CO}(observed)/N_{CO}(modeled)$

[b]Predicted using $N_{HCN}(observed)/N_{HCN}(modeled)$

Note. — Predicted column densities were calculated from modeling done by Aikawa & Herbst (2001) and the observations of Qi (2001)

from $C^{18}O$ 1-0. This difference may be related to the fact that CO is better predicted by Aikawa et al. (2002) for the observed sources than CN and HCN. They suggest that this can be rectified by including the dissociation of CO by interstellar and stellar UV radiation, resulting in increased atomic carbon, and thus CN, in photodissociation regions. This would also result in increased abundances of HDO, since HDO is deuterated through reactions involving H_2D^+, which is destroyed by CO. The treatment of CO photodissociation in the model will have a large effect on the relationship between the predicted CO and HDO (and CO and CN) column densities. Thus, scaling the modeled column densities by HCN more correctly predicts the HDO column densities than does scaling by CO.

4.5 D/H ratios

The ratios of the column densities of deuterated and hydrogenated species are presented in Table 4.5. We have not included $(D/H)_{H_2O}$ for HD 163296 or MWC 480 because we did not detect HDO in these sources and there are no previous observations of water in these disks. The $(D/H)_{H_2O}$ for LkCa 15 is calculated using the predicted column densities for H_2O from the previous section, scaling by the ratio of the observed-to-modeled HCN abundances. The $(D/H)_{DCN}$ ratios are calculated directly from the observed HCN upper limits (for HD 163296) or $H^{13}CN$ abundances (for LkCa 15). We have added the $(D/H)_{HCO^+}$ ratio obtained for the face on disk around the T Tauri star TW Hya (van Dishoeck et al., 2003) to the table for comparison. $(D/H)_{HCO^+}$ in TW Hya is similar to $(D/H)_{H_2O}$ in LkCa 15 and $(D/H)_{HCN}$ in HD 163296, but quite different from $(D/H)_{HCN}$ in LkCa 15. This can be explained by differences in the formation mechanisms of these deuterated species. $(D/H)_{HCO^+}$ and $(D/H)_{H_2O}$ can be expected to be similar in the two T Tauri star disks, because both DCO^+ and HDO are deuterated through H_2D^+ via the highly temperature-dependent reaction,

$$H_3^+ + HD \rightleftharpoons H_2D^+ + H_2 \qquad \Delta E = 230\ K \tag{4.24}$$

At warm temperatures, the reverse reaction becomes more important, and as H_2D^+ is destroyed and $(D/H)_{H_2O}$ and $(D/H)_{HCO^+}$ decrease (Aikawa & Herbst, 2001). $(D/H)_{H_2O}$ and $(D/H)_{HCO^+}$ are also highly dependent on the presence of X-rays and gas-phase CO and H_2, which destroy H_2D^+ (Aikawa & Herbst, 1999). So, for sources with similar conditions (temperature, depletion, etc.) we would expect the $(D/H)_{HCO^+}$ and $(D/H)_{H_2O}$ ratios to be similar. DCN, however, is formed via mechanisms that are very different then the formation of HDO and DCO^+. The major formation pathways of DCN are the reactions of D and H_2CN on grain surfaces and of CH_2D^+ and N in the gas phase, following grain-surface formation of CH_4 or CH_3. The production of DCN is therefore tied to chemistry on, and desorption from, grain surfaces. DCN is also formed by the reaction of N with CHD and HCN via the reaction of N with CH_2. Because the CH_2 is formed more quickly than CHD, $(D/H)_{HCN}$ is also believed to be strongly dependent on the disk age (Aikawa & Herbst, 1999). All of these mechanisms indicate that $(D/H)_{HCN}$ should increase with moderate increases in temperature as $(D/H)_{H_2O}$ and $(D/H)_{HCO^+}$ decrease. The larger $(D/H)_{HCN}$ ratios in the HD 163296 disk (and perhaps also the non-detection of HDO toward this disk) with respect to the K star LkCa 15 may be explained by differing stellar luminosities and hence disk temperatures.

The D/H ratios in the two disks can be compared to those of molecular clouds, hot cores and our solar system. The ratios vary slightly from disk-to-disk and lie within the range of D/H ratios found in molecular clouds and hot cores. All four of these D/H ratios are much larger than that of the early solar nebula (10^{-5}) and consistent with deuterium abundances in comets. Therefore, conclusions from previous observations, which stated that comets were assembled from interstellar material, can

Table 4.5. D/H ratios in disks.

Star	molecule	D/H
LkCa 15	HCN	<0.001
-	H_2O	0.0001–0.064
HD 163296	HCN	>0.094
TW Hya	HCO^+	0.035

Note. — The upper limit for $(D/H)_{H2O}$ was calculated from model abundances of H_2O (Aikawa & Herbst, 2001) scaled by ratios of observed-to-modeled HCN abundances. The lower limit for $(D/H)_{H2O}$ was calculated from nondetections of $H_2{}^{18}O$ using OVRO.

be adapted to state that comets could be formed in or with material that passed through the outer regions of disks where the conditions are more similar to interstellar clouds than nebular regions near proto-Jovian planets.

4.6 Image modeling

Molecular distributions are essential to understanding the chemistry taking place in disks. The HDO emission observed here, as well as previous observations toward LkCa 15 (Qi, 2001), indicates large differences in the morphology of the emission in the integrated intensity maps (Figure 4.5). CO and HCO^+ emission peak at the source position while the HCN, CN and HDO emission peak approximately 2″ away along the major axis of the disk. This is especially interesting because the spectra for CO 2-1, HCO^+, HDO and HCN do not differ significantly. Lack of emission toward the star results in only small changes to the line wings, which are buried in the noise in the HDO spectrum, but may be slightly more visible in the higher signal-to-noise HCN spectrum. Clearly, imaging is necessary to study this type of disk structure and there is a need for detailed models which can be used to reproduce and interpret these images.

For this reason we have created a model to simulate our observed channel maps and images of protoplanetary disks (see Chapter 2). The temperature and hydrogen density distributions are determined using physically self-consistent disk models of D'Alessio et al. (2001), assuming a power law distribution of dust sizes ($n(a) = a^{-3.5}$), an accretion rate of 10^{-8} $M_\odot$/yr and equal dust and gas temperatures. The stellar parameters are specific for LkCa 15 ($M_* = 1.0$ $M_\odot$, $R_* = 1.64$ $R_\odot$, $T_* = 4395$ K). The resulting physical disk model is then combined with the distribution of the

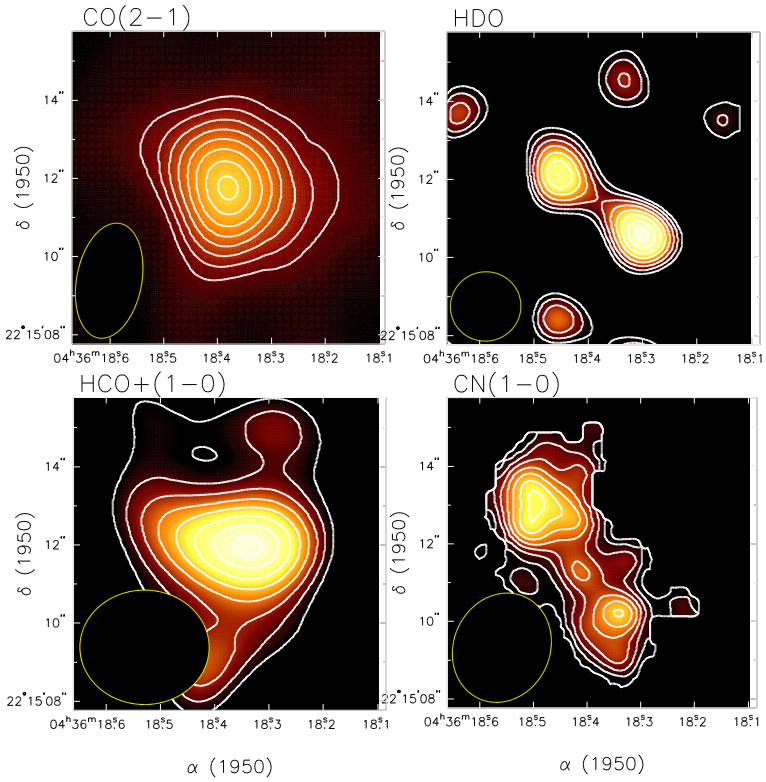

Figure 4.5 OVRO observations of CO (kindly provided by Koerner and Sargent), HDO, HCO^+ and HCN toward the T Tauri star LkCa 15. While CO and HCO^+ are centered at the stellar position, CN, HDO and HCN (not shown) peak $\sim 2''$ away.

molecule of interest and the radiation transfer in the disk is calculated using a non-LTE Monte Carlo code (Hogerheijde & van der Tak 2001). The input parameters for this model are the mass and inclination of the disk, determined from previous observations of the continuum and CO emission toward this source (Beckwith et al., 1990, Duvert et al., 2000). The inner and outer radius of the disk (R_{out} = 430 AU) and turbulent velocity width (0.1 km/s) are parameters which are adjusted to fit our observed CO 2-1 emission spectrum (Qi et al., 2003). The initial results of our model are equivalent to the observations of a telescope with essentially infinite resolution and complete (u, v) coverage. The map is then convolved with the (u, v) sampling obtained, in order to simulate the OVRO observations more explicitly. We will now use these models to interpret our HCN and HDO observations.

The chemical models of Aikawa & Herbst (2001) and Willacy & Langer (2000) suggest that the radial distribution of HCN and CN in disks is determined by the processes of photodissociation by interstellar and stellar UV combined with desorption from grain surfaces. The newest models (Aikawa et al., 2002) suggest that the competition between interstellar and stellar UV in particular determine the variation in the amount of HCN as a function of radius. We simulate the emission morphology discussed above by concentrating the HCN in a ring around the star. We use a simple

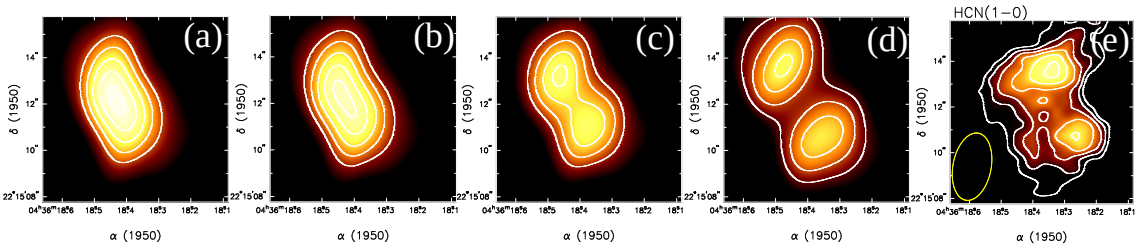

Figure 4.6 Model fits to the HCN J = 1-0 emission from LkCa 15. The observed HCN emission (e) is compared to a model of an annulus of HCN with an outer radius of 400 AU and an inner radius of 50 (a), 100 (b), 200 (c) and 300 AU (d). In each case, the total flux of the model image is set to match the observed HCN map. The observed emission is consistent with an inner radius between 200 AU and 300 AU (i.e., between (c) and (d)).

model, with an outer region in which the column density is constant and the volume density is proportional to that of hydrogen and an inner region in which the column density is zero. We then set the outer radius of the annulus to the disk radius as determined from the CO 2-1 observations (∼430 AU) and vary the inner radius to match the observed integrated intensity maps. In each case the column density of HCN in the ring is set by matching the integrated flux of the modeled map to that observed. As we vary the inner radius we can see that these models can reproduce the structure of the HCN emission only with large depletion zones in the disk center ($R_i \sim$ 200–300 AU). More realistic models that incorporate radial gradients in molecular abundances will be used in the future to simulate the combined effects of desorption from grains and photodissociation of HCN from interstellar and stellar UV.

Although we have not yet modeled the HDO emission, the observed double-peaked emission map may also result from a ring-like distribution (or a steep gradient). Here models suggest that the annulus could be formed due to reduced production of HDO near the star as H_2D^+, the primary precursor to HDO, is created less efficiently due to the increasing temperature gradient in the inner disk. This causes the HDO abundance to peak at R≈250 AU (Aikawa & Herbst, 2001), and as the previous HCN models show, this morphology is consistent with the observed emission.

4.7 Future observations

The observations presented here are severely limited by the sensitivity of current millimeter arrays, especially in the 1 mm window. Although these disks were chosen because of previously observed strong emission from several molecular lines at 3 mm, the observed emission from deuterated species is very weak, on the order of 1.5–3σ for all deuterated molecules, and HDO in HD 163296 and MWC 480 and DCN in LkCa 15 were not detected. From this analysis, it is clear that detailed study of deuteration in disks requires either observations of the same deuterated/hydrogenated molecule in several disks or observations of several deuterated species in a single source. Due to the

non-detections of HCN in HD 163296 and DCN in LkCa 15, the D/H ratios obtained represent only lower and upper limits, respectively. Additionally, because water has not been observed toward these three sources, the calculation of the $(D/H)_{H_2O}$ and the interpretation of HDO observations depend largely on model predictions for water abundances. Future millimeter arrays, such as ALMA, will offer vast improvements in sensitivity, and will undoubtedly make studies such as those presented here obsolete. In the near future, the Combined Array for Research in Millimeter Astronomy (CARMA) will make these studies much more efficient. For example, the observations of HDO in LkCa 15 presented here, which represents approximately 40 hours of observing time with OVRO, could be done in 5 hours with CARMA[2].

Although future arrays offer promise for the study of deuterium enrichment in disks, the next step for these studies can be pursued with current instrumentation. Water and HCN (as well as their isotopomers) are frozen out onto grain surfaces in the midplane of disks and therefore the observations of HDO and DCN presented here only serve as an effective probe of D/H ratios in disk surface layers. Observations of molecules that are believed to remain in the gas phase within the disk midplane, specifically ions (DCO^+, N_2D^+ and H_2D^+) can be used to probe planet forming regions. Additionally, D/H ratios are predicted to be much higher in the disk midplane as molecules which typically react to destroy these ions are depleted onto grain surfaces. DCO^+ is a good candidate for millimeter observations because, HCO^+ has been readily observed in large quantities in disks (Qi, 2001; this thesis), and predict column densities of DCO^+ on the order of 10^{12} cm^{-2}. Additionally, as mentioned earlier, DCO^+ has already been observed in the circumstellar disks around TW Hya and, more recently, DM Tau in single dish observations at the JCMT (Thi et al., 2001) and IRAM 30m telescope (Dutrey, 2003). Observations of N_2H^+ with OVRO (Qi et al., 2003) suggest N_2D^+ column densities of $\sim 10^{11}$ cm^{-2}. H_2D^+, which is an isotopomer of H_3^+, the most abundant ion and the cornerstone of ion-molecule chemistry, resides in the ground para state at typical disk midplane temperatures. The strongest transition of H_2D^+ in disks lies at 1370 GHz, and is an excellent project for the CASIMIR instrument on SOFIA. The calculation of HDO/H_2O ratios in our study was limited by the lack of H_2O detections in disks. This will soon be remedied by the HIFI instrument on Herschel, which will be used to perform an extensive survey of strong H_2O lines in many sources, including planet-forming disks.

4.8 Summary

We present the first observations of DCN and HDO toward circumstellar disks. Images of HDO in the T Tauri star LkCa 15 show emission which is consistent with an annulus of inner radius 200 AU and outer radius 400 AU. This is consistent with our current understanding of disk chemistry,

[2] *http://www.mmarray.org*

which suggests that the HDO distribution is actually a gradient as a function of distance from the star and peaks at ∼300 AU. The sensitivity of the observed morphology to the steepness of this gradient will be further explored in future work. D/H ratios in disks, including those reported here along with observations of DCO^+ toward the T Tauri star TW Hya, are similar to that of hot cores and molecular clouds and comets, which is consistent with comet formation in the outer regions of disks. Future observations of deuterated ions (H_2D^+ and N_2D^+) should probe much closer to the disk midplane and constrain the deuteration in these regions. With more sensitive, high-resolution arrays such as CARMA and ALMA, we will be able to expand our studies to include more molecules and probe the inner, planet-forming regions of circumstellar disks.

Bibliography

Aikawa, Y. & Herbst, E. 1999, ApJ, 526, 314

—. 2001, A&A, 371, 1107

Aikawa, Y., Umebayashi, T., Nakano, T., & Miyama, S. M. 1999, ApJ, 519, 705

Aikawa, Y., van Zadelhoff, G. J., van Dishoeck, E. F., & Herbst, E. 2002, A&A, 386, 622

Beckwith, S. V. W. & Sargent, A. I. 1996, Nature, 383, 139

Beckwith, S. V. W., Sargent, A. I., Chini, R. S., & Guesten, R. 1990, AJ, 99, 924

Bockelée-Morvan, D., Gautier, D., Lis, D. C., Young, K., Keene, J., Phillips, T., Owen, T., Crovisier, J., Goldsmith, P. F., Bergin, E. A., Despois, D., & Wooten, A. 1998, Icarus, 133, 147

Brown, P. D., Charnley, S. B., & Millar, T. J. 1988, MNRAS, 231, 409

Brown, P. D. & Millar, T. J. 1989, MNRAS, 237, 661

Chiang, E. I. & Goldreich, P. 1997, ApJ, 490, 368

D'Alessio, P., Calvet, N., & Hartmann, L. 2001, ApJ, 553, 321

D'Alessio, P., Calvet, N., Hartmann, L., Lizano, S., & Cantó, J. 1999, ApJ, 527, 893

Dartois, E., Dutrey, A., & Guilloteau, S. 2003, A&A, 399, 773

Deloule, E., Doukhan, J.-P., & Robert, F. 1997, in Lunar and Planetary Institute Conference Abstracts, 291

Drouart, A., Dubrulle, B., Gautier, D., & Robert, F. 1999, Icarus, 140, 129

Duncan, M., Quinn, T., & Tremaine, S. 1988, ApJ, 328, 69

Dutrey, A. 2003, in Proceedings of the IAU, Star Formation at High Angular Resolution, in press

Dutrey, A., Guilloteau, S., & Guelin, M. 1997, A&A, 317, L55

Duvert, G., Guilloteau, S., Ménard, F., Simon, M., & Dutrey, A. 2000, A&A, 355, 165

Eberhardt, P., Reber, M., Krankowsky, D., & Hodges, R. R. 1995, A&A, 302, 301

Fernandez, J. A. & Ip, W.-H. 1991, in ASSL Vol. 167: IAU Colloq. 116: Comets in the post-Halley era, 487–535

Festou, M. C., Rickman, H., & West, R. M. 1993, A&A Rev., 4, 363

Finocchi, F., Gail, H.-P., & Duschl, W. J. 1997, A&A, 325, 1264

Gautier, D. & Morel, P. 1997, A&A, 323, L9

Geiss, J. & Reeves, H. 1981, A&A, 93, 189

Gensheimer, P. D., Mauersberger, R., & Wilson, T. L. 1996, A&A, 314, 281

Goldsmith, P. F., Langer, W. D., & Velusamy, T. 1999, ApJ, 519, 173

Guilloteau, S. & Dutrey, A. 1998, A&A, 339, 467

Hayashi, C. 1981, Progress of Theoretical Physics Supplement, 70, 35

Helmich, F. P., van Dishoeck, E. F., & Jansen, D. J. 1996, A&A, 313, 657

Jacq, T., Walmsley, C. M., Henkel, C., Baudry, A., Mauersberger, R., & Jewell, P. R. 1990, A&A, 228, 447

Kuiper, G. P. 1951, in Proceedings of a topical symposium, commemorating the 50th anniversary of the Yerkes Observatory and half a century of progress in astrophysics, New York: McGraw-Hill, 1951, edited by Hynek, J.A., 357

Linsky, J. L., Diplas, A., Wood, B. E., Brown, A., Ayres, T. R., & Savage, B. D. 1995, ApJ, 451, 335

Linsky, J. L. & Wood, B. E. 1996, ApJ, 463, 254

Mangum, J. G., Plambeck, R. L., & Wooten, A. 1991, ApJ, 369, 169

Mannings, V. & Sargent, A. I. 1997, ApJ, 490, 792

—. 2000, ApJ, 529, 391

Meier, R., Owen, T. C., Jewitt, D. C., Matthews, H. E., Senay, M., Biver, N., Bockelee-Morvan, D., Crovisier, J., & Gautier, D. 1998a, Science, 279, 1707

Meier, R., Owen, T. C., Matthews, H. E., Jewitt, D. C., Bockelee-Morvan, D., Biver, N., Crovisier, J., & Gautier, D. 1998b, Science, 279, 842

Millar, T. J., Bennett, A., & Herbst, E. 1989, ApJ, 340, 906

Mumma, M. J., Dello Russo, N., DiSanti, M. A., Magee-Sauer, K., Novak, R. E., Brittain, S., Rettig, T., McLean, I. S., Reuter, D. C., & Xu, L. 2001, Science, 292, 1334

Nesbitt, F., Marston, G., & Stief, L. 1990, J. Phys. Chem., 94, 4946

Pickett, H. M., Poynter, R. L., Cohen, E. A., Delitsky, M. L., Pearson, J. C., & Muller, H. S. P. 1998, Journal of Quantitative Spectroscopy and Radiative Transfer, 60, 883

Piskunov, N., Wood, B. E., Linsky, J. L., Dempsey, R. C., & Ayres, T. R. 1997, ApJ, 474, 315

Qi, C. 2001, PhD thesis, California Institute of Technology

Qi, C., Kessler, J. E., Koerner, D. W., Sargent, A. I., & Blake, G. A. 2003, ArXiv Astrophysics e-prints

Rodgers, S. D. & Charnley, S. B. 2002, Planet. Space Sci., 50, 1125

Sault, R. J., Teuben, P. J., & Wright, M. C. H. 1995, in ASP Conf. Ser. 77: Astronomical Data Analysis Software and Systems IV, 433–+

Scoville, N. Z., Carlstrom, J. E., Chandler, C. J., Phillips, J. A., Scott, S. L., Tilanus, R. P. J., & Wang, Z. 1993, PASP, 105, 1482

Simon, M., Dutrey, A., & Guilloteau, S. 2001, ApJ, 545, 1034

Thi, W. F., van Dishoeck, E. F., Blake, G. A., van Zadelhoff, G. J., Horn, J., Becklin, E. E., Mannings, V., Sargent, A. I., van den Ancker, M. E., Natta, A., & Kessler, J. 2001, ApJ, 561, 1074

van Dishoeck, E. F., Thi, W.-F., & van Zadelhoff, G.-J. 2003, A&A, 400, L1

van Zadelhoff, G.-J., van Dishoeck, E. F., Thi, W.-F., & Blake, G. A. 2001, A&A, 377, 566

Walmsley, C. M., Hermsen, W., Henkel, C., Mauersberger, R., & Wilson, T. L. 1987, A&A, 172, 311

Weaver, H. A., Chin, G., Bockelée-Morvan, D., Crovisier, J., Brooke, T. Y., Cruikshank, D. P., Geballe, T. R., Kim, S. J., & Meier, R. 1999, Icarus, 142, 482

Willacy, K. & Langer, W. D. 2000, ApJ, 544, 903

Wilson, T. L. & Rood, R. 1994, ARA&A, 32, 191

Wootten, A. 1987, in IAU Symp. 120: Astrochemistry, Vol. 120, 311–318